NOTES AND CORRESPONDENCE

Ellipse-Fitting Techniques Applied to 2D-PMS Raindrop Images

RONGRUI XIAO, V. CHANDRASEKAR, AND DAVID GARBRICK

Colorado State University, Fort Collins, Colorado

1 May 1994 and 1 May 1995

ABSTRACT

An ellipse-fitting technique is introduced in this paper to process the images of raindrops sampled by a 2D-PMS (Particle Measuring Systems, Inc.) probe. Algorithms to estimate size, shape, and orientation parameters of partial raindrop images are presented. This technique is evaluated by fitting full raindrop images and comparing the results with other procedures such as Fourier descriptor and moment descriptor methods. It is also evaluated by applying this procedure to partial raindrop images constructed by truncating the top part or the bottom part of full raindrop images, while at the same time the estimates obtained from the full images are used for comparison against the estimates from partial images. It is shown that the ellipse-fitting technique is a viable tool for processing complete 2D-PMS raindrop images, and more importantly, this technique works successfully for processing partial raindrop images. Results of 2D-PMS data analysis of side-looking raindrop images collected during the CaPE (Convection and Precipitation/Electrification) field program are presented.

1. Introduction

With the advent of polarimetric weather radar, several field programs such as the Cooperative Convective Precipitation Experiment (CCOPE 1981), the Joint Airport Weather Study (JAWS 1982), the May Polarization Experiment (MAYPOLE 1983) and the Convection and Precipitation/Electrification Experiment (CaPE 1991) have been conducted to address the problems of quantitative precipitation estimation and hydrometeor phase identification. In situ measurements were made by instrumented aircraft equipped with 2D-PMS (Particle Measuring Systems, Inc.) probes (Knollenberg 1981) during most of the above field experiments. The 2D-PMS probes were mounted vertically in several field experiments such that the top view of the hydrometeors was captured in the shadowgraph images that were produced. Cooper (1980) developed a "circle-fit" algorithm to size the circular images obtained from the vertically oriented optical probes. This circle-fit algorithm and other related procedures have been extensively used to obtain geometric parameters such as size and center of the sampled hydrometeors, which were subsequently used to obtain particle size distribution and concentration. This procedure became an important part of several hydrometeor processing algorithms (Heymsfield and Parrish 1979; Hemysfield and Baumgardner 1985) used with top-looking 2D-PMS images.

Since the advancement of polarimetric radar techniques for remote sensing of precipitation, the knowledge of the hydrometeor shapes obtained from side-looking observations has become important. The 2D-PMS probes can be rotated 90° to capture the horizontal images of particles, and the observations of the side and top views of raindrops show that they can be approximated by oblate spheroidal shapes (Bringi et al. 1984; Chandrasekar et al. 1988). The side-looking images of raindrops have been used to obtain shape information such as axis ratio and canting angle (Bringi et al. 1984; Chandrasekar et al. 1988). However, to obtain information on drop size distribution (DSD) or rainfall rate, we need to know the number of particles in each size bin that fall inside the sampling volume. An example of raindrop images collected by the 2D-PMS probes is shown in Fig. 1. This sample, like all others, contains many partial images. In order to compute the number concentration, we can use the approach of counting only the drops that are fully in the sampling area, however, this procedure decreases the sampling volume of large drops to unusable values. Sampling of large drops are important since they contribute significantly to reflectivity Z_H and differential reflectivity Z_{DR} computations. The larger the size of a raindrop, the greater the chance that it will produce a partial image. Therefore, there is an important need to reconstruct the full images of raindrops based on the partial observed images.

Corresponding author address: Dr. V. Chandrasekar, Department of Electrical Engineering, Colorado State University, Fort Collins, CO 80523.

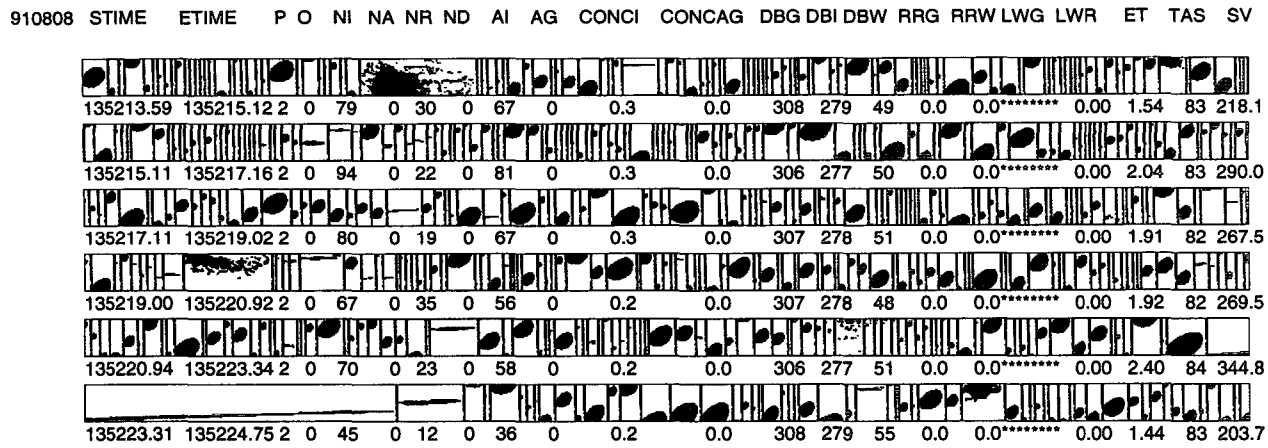

FIG. 1. Several records of side-looking 2D-P raindrop images collected by the Wyoming King Air on 8 August 1991 during CaPE. Note the partial raindrop images, located at the top or the bottom of the sampling area.

Fourier and moment descriptor methods have been used successfully to analyze full 2D-PMS images (Rahman et al. 1981; Duroure 1982; Hunter et al. 1984; Chandrasekar et al. 1990), but both procedures are not applicable for partial images. Application of curve-fitting procedures such as the one used by Cooper (1980) for side-looking raindrop images is very complex analytically and computationally. This is because an arbitrary ellipse has five unknowns (the x, y coordinates of the center, the semimajor and semiminor axes, and the orientation angle) related by a nonlinear trigonometric equation [see Eq. (1)]. We introduce an ellipse-fitting technique in this paper, which is designed for ease of usage with the natural 2D-PMS data acquisition process. The technique estimates the center of a raindrop image first and then subsequently obtains all the other parameters of the raindrop. Because only a part of the contour is needed for the ellipse-fitting process, this technique works well for both full and partial raindrop images.

Our paper is organized as follows. Section 2 describes the ellipse-fitting algorithms along with pertinent equations. In section 3, we evaluate the algorithms developed in section 2 using data collected during the CaPE field program. Section 4 demonstrates the application of this data analysis procedure for obtaining raindrop size concentrations. Section 5 summarizes the key results of this paper.

2. Technique description

a. Shapes of raindrops

Many studies on the shape of raindrops suggest that the shapes of raindrops can be approximated by oblate spheroids whose side views are elliptical (Bringi et al. 1984; Beard and Chuang 1987; Chandrasekar et al. 1988). Therefore, the parameters of a free-falling raindrop, such as size, shape, and orientation, can be associated with the parameters of an ellipse. A brief description of the parameters of a general ellipse is very useful in defining the estimators of raindrop parameters.

b. Properties of a general ellipse

1) GENERAL EQUATION

The general equation of an ellipse with arbitrary origin and canting angle is given by

$$\frac{[(x - x_c)\cos\alpha + (y - y_c)\sin\alpha]^2}{a^2} + \frac{[(x - x_c)\sin\alpha - (y - y_c)\cos\alpha]^2}{b^2} = 1, \quad (1)$$

where (x_c, y_c) is the center of the ellipse, a and b are the semimajor axis and semiminor axis, respectively, and α is the canting angle measured from the X axis. Based on this general equation, we can obtain several useful formulas related to the estimation of the parameters of the ellipse.

The natural order in which data are collected and recorded on hydrometeor images is in scan lines that are parallel to each other. The diode array as it scans an image also provides horizontal parallel lines intersecting the contour of the image. Most of the expressions developed in this paper are based on these parallel lines. This type of analysis simplifies the processing algorithm to a large extent because it conforms to the data collection procedure.

2) COORDINATES OF THE CENTER

If we have the knowledge of the center coordinates of an ellipse, we can translate all coordinates of the contour of the ellipse with respect to the center and thus simplify (1) considerably. Therefore, the center of the ellipse is the first natural parameter of interest. In addition, the knowledge of the center of a raindrop image is important to decide if the center of the raindrop is within the sampling volume or not, for com-

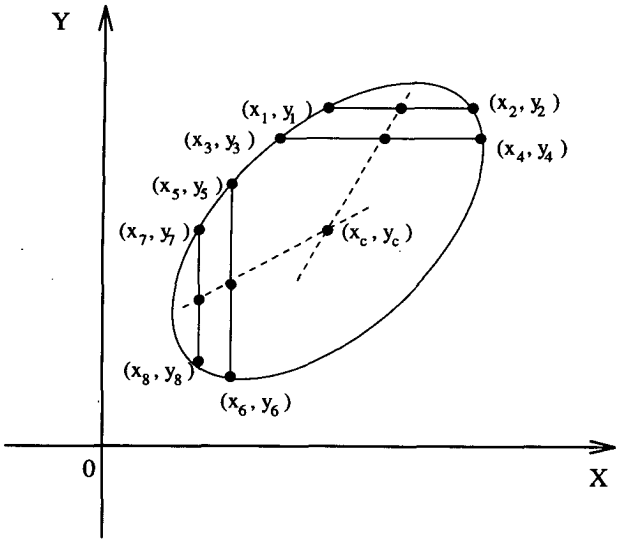

FIG. 2. Diagram showing the technique to find the center of an ellipse. It is obtained as the intersection point of the (dashed) lines passing through the midpoints of two pairs of parallel lines intersecting the boundary.

putations such as concentration. Figure 2 shows the diagram of an arbitrarily oriented ellipse. The procedure for estimating the center is as follows (see the appendix for details of the proof).

(i) Two pairs of parallel lines are selected, namely line 1 that passes through (x_1, y_1), (x_2, y_2) and line 2 that passes through (x_3, y_3), (x_4, y_4) on the ellipse; line 3 that passes through (x_5, y_5), (x_6, y_6) and line 4 that passes through (x_7, y_7), (x_8, y_8) on the ellipse. Note that coordinates (x_1, y_1) to (x_8, y_8) are points of intersection between the parallel lines and the contour of the ellipse. The slopes of the four lines, s_1, s_2, s_3, s_4, respectively, can be expressed as

$$s_1 = \frac{y_2 - y_1}{x_2 - x_1} = s_2 = \frac{y_4 - y_3}{x_4 - x_3} \tag{2}$$

$$s_3 = \frac{y_6 - y_5}{x_6 - x_5} = s_4 = \frac{y_8 - y_7}{x_8 - x_7}, \tag{3}$$

but $s_1 \neq s_3$, which implies that line 1 parallels line 2 and line 3 parallels line 4, but the pairs of lines are not parallel to each other.

(ii) The coordinates of the midpoints of line 1, line 2, line 3, and line 4 inside the ellipse are obtained as

$$x_{c1} = \frac{x_1 + x_2}{2}, \quad y_{c1} = \frac{y_1 + y_2}{2} \tag{4}$$

$$x_{c2} = \frac{x_3 + x_4}{2}, \quad y_{c2} = \frac{y_3 + y_4}{2} \tag{5}$$

$$x_{c3} = \frac{x_5 + x_6}{2}, \quad y_{c3} = \frac{y_5 + y_6}{2} \tag{6}$$

$$x_{c4} = \frac{x_7 + x_8}{2}, \quad y_{c4} = \frac{y_7 + y_8}{2}. \tag{7}$$

(iii) Another set of two lines are selected, one passes through (x_{c1}, y_{c1}), (x_{c2}, y_{c2}) and the other passes through (x_{c3}, y_{c3}), (x_{c4}, y_{c4}). Then the intersection point of these two lines, (x_c, y_c), gives the center point of the ellipse. Let

$$k_1 = \frac{y_{c2} - y_{c1}}{x_{c2} - x_{c1}}, \quad k_2 = \frac{y_{c4} - y_{c3}}{x_{c4} - x_{c3}} \tag{8}$$

and $k_1 \neq k_2$, then

$$x_c = \frac{(y_{c2} - y_{c4}) - (k_1 x_{c2} - k_2 x_{c4})}{k_2 - k_1} \tag{9}$$

$$y_c = \frac{(k_2 y_{c2} - k_1 y_{c4}) - k_1 k_2 (x_{c2} - x_{c4})}{k_2 - k_1}. \tag{10}$$

3) ESTIMATION OF PARAMETERS

(i) *Canting angle and axis ratio*

Once we obtain the location of the center of the ellipse, we can transform the origin of the coordinate system to the center of the ellipse. Since the canting angle and axis ratio of the ellipse are shift invariant, they can be easily obtained from the contour points of the shifted ellipse.

Consider a canted ellipse centered at the origin (0, 0) as shown in Fig. 3. Let L_v be the vertical line that passes through points (x_{s1}, y_{s1}), (x_{s2}, y_{s2}) on the contour of the ellipse with $x_{s1} = x_{s2}$ and let L_h be a horizontal line that passes through points (x_{s5}, y_{s5}), (x_{s6}, y_{s6}) on the contour of the ellipse with $y_{s5} = y_{s6}$, as shown in Fig. 3. Let

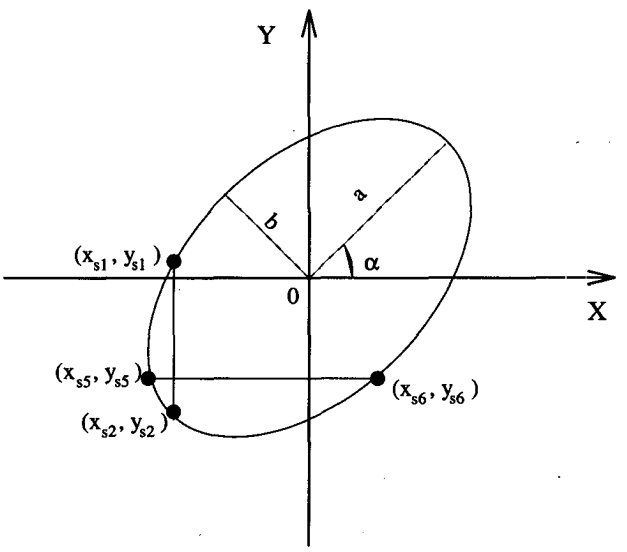

FIG. 3. Diagram showing the procedure to compute the canting angle α and axis ratio r for an ellipse with center at the origin. Canting angle α and axis ratio r are computed from the coordinates of intersections of the ellipse with a vertical line and a horizontal line.

$$d_1 = \frac{x_{s1}}{y_{s1} + y_{s2}} \tag{11}$$

$$d_2 = \frac{y_{s5}}{x_{s5} + x_{s6}}. \tag{12}$$

We can show that (see the appendix) the canting angle and the axis ratio satisfy the following equations:

$$\alpha = \frac{1}{2}\tan^{-1}\left(\frac{1}{d_1 - d_2}\right) \tag{13}$$

$$r = \frac{b}{a} = \left[\frac{(d_1 + d_2)\sin 2\alpha - 1}{(d_1 + d_2)\sin 2\alpha + 1}\right]^{1/2}. \tag{14}$$

(ii) *Semimajor and semiminor axes*

The semimajor axis a and the semimini axis b can be easily calculated using the general equation of the ellipse after we get the center location (x_c, y_c), the canting angle α, and the axis ratio r using the following equations:

$$a = \{[(x - x_c)\cos\alpha + (y - y_c)\sin\alpha]^2 + \frac{1}{r^2}[(x - x_c)\sin\alpha - (y - y_c)\cos\alpha]^2\}^{1/2} \tag{15}$$

$$b = ra. \tag{16}$$

Note that it is easy to find data points on either a full or a partial 2D-PMS raindrop image corresponding to vertical and horizontal directions that cross the image contour, as shown in Fig. 5. Since we only need a few points instead of the complete contour of the ellipse to get all above estimates, this method is readily suitable for the partial images.

c. Ellipse-fitting algorithm

In section 2b, we have developed formulas for the estimation of parameters for raindrop images. Both complete and partial images can be processed using the method descripted in previous section. In general, partial 2D-PMS images occur at the top or the bottom of the scan region of the optical probe array. Therefore, partial images are formed with their top parts or bottom parts truncated. Figure 4 shows two typical partial 2D-PMS raindrop images.

It is shown in section 2b that we can estimate the center position and the other parameters of an ellipse by using only a few points on its contour. The accuracy of the estimates can be improved by using more points to obtain several estimates and averaging them. Since we do not have many available data points on a real PMS image, especially a partial image, we need to use as many as possible of them to get reasonably accurate estimates. The ellipse-fitting algorithm is summized below (see Fig. 5).

Step 1: Arrange the input contour data.

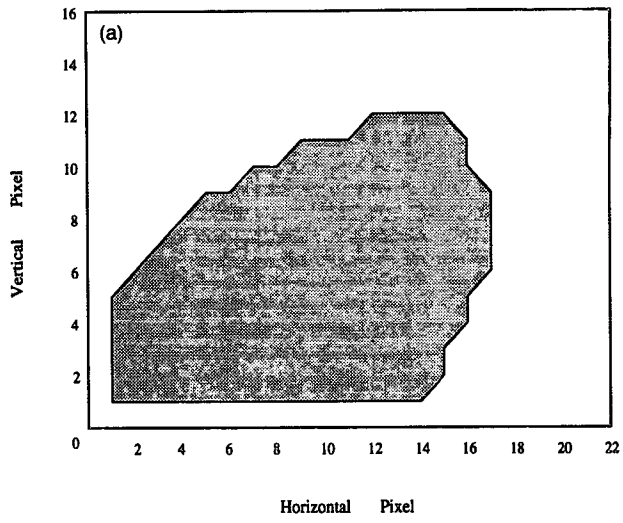

FIG. 4. Two typical examples of partial raindrop images. (a) The bottom part of the image is truncated. (b) The top part of the image is truncated.

From the quantized contour of the partial raindrop image, obtain all datapoint pairs corresponding to lines paralleling axis X or axis Y and order them in two groups separately as

group 1—(lines paralleling X axis)

$$\begin{array}{lll} (x_{i1}, y_{i1}), & (x_{i2}, y_{i2}), & y_{i1} = y_{i2} \\ (x_{i3}, y_{i3}), & (x_{i4}, y_{i4}), & y_{i3} = y_{i4} \\ \vdots & \vdots & \vdots \\ (x_{im}, y_{im}), & (x_{im+1}, y_{im+1}), & y_{im} = y_{im+1} \end{array}$$

group 2—(lines paralleling Y axis)

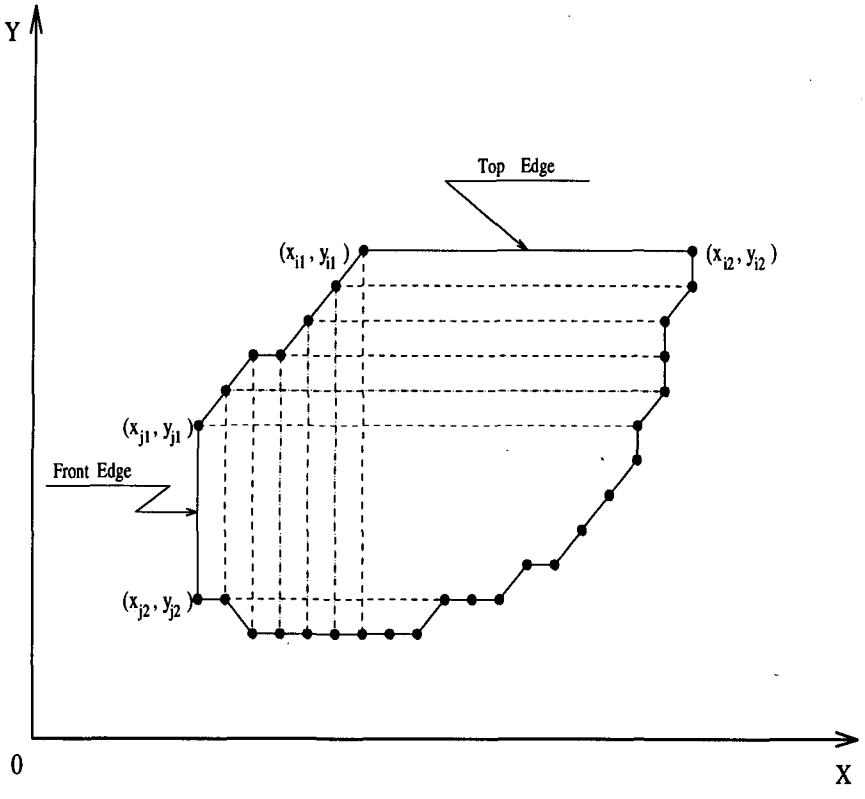

FIG. 5. All possible vertical and horizontal parallel lines intersecting the contour of the ellipse shown for a typical partial image.

$$\begin{array}{lll} (x_{j1}, y_{j1}), & (x_{j2}, y_{j2}), & x_{j1} = x_{j2} \\ (x_{j3}, y_{j3}), & (x_{j4}, y_{j4}), & x_{j3} = x_{j4} \\ \vdots & \vdots & \vdots \\ (x_{jn}, y_{jn}), & (x_{jn+1}, y_{jn+1}), & x_{jn} = x_{jn+1}. \end{array}$$

Step 2: Estimation of the center of the raindrop image.

One pair of lines in group 1 and another pair of lines in group 2 are chosen and then the procedure described in (2)–(10) is applied to get one estimate of the coordinates of the ellipse center $(\hat{x}_{ck}, \hat{y}_{ck})$. This process is repeated by using all different line pair combinations in group 1 and group 2 to get a group of estimates. Let K be the total number of combinations, then estimates are averaged to get the final estimate of the center position of the ellipse as

$$\bar{x}_c = \frac{1}{K} \sum_k \hat{x}_{ck} \tag{17}$$

$$\bar{y}_c = \frac{1}{K} \sum_k \hat{y}_{ck}. \tag{18}$$

Step 3: Estimation of the canting angle and the axis ratio.

One line in group 1 and another in group 2 are chosen and then the coordinates are transformed with respect to $(\bar{x}_c, \bar{y}_c)$, the center, to make $(\bar{x}_c, \bar{y}_c)$ the new origin. Subsequently (13) and (14) are used to get the estimates of the canting angle $\hat{\alpha}_l$ and the axis ratio $\hat{r}_l$. This process is repeated for all combinations of lines in group 1 and group 2. The final estimates of the canting angle and the axis ratio are obtained by averaging all above estimates separately. Based on the estimates of (x_c, y_c), α, r, we apply all available contour points of the ellipse to (15) and (16) to get a group of estimates for a and b. These estimates are averaged to get the final estimates for a and b.

3. Performance evaluation

a. Ellipse-fitting techniques for full raindrop images

As mentioned above, Fourier and moment methods have been used successfully for processing full 2D-PMS images of raindrops to estimate their size, shape, and orientation. Therefore, for evaluation purposes we can compare the ellipse-fitting algorithm introduced here against the Fourier and moment descriptor techniques. Chandrasekar et al. (1990) showed that Fourier and moment methods estimates agree very well between each other. Therefore, comparison with Fourier descriptor estimates are similar to the comparison with moment descriptors.

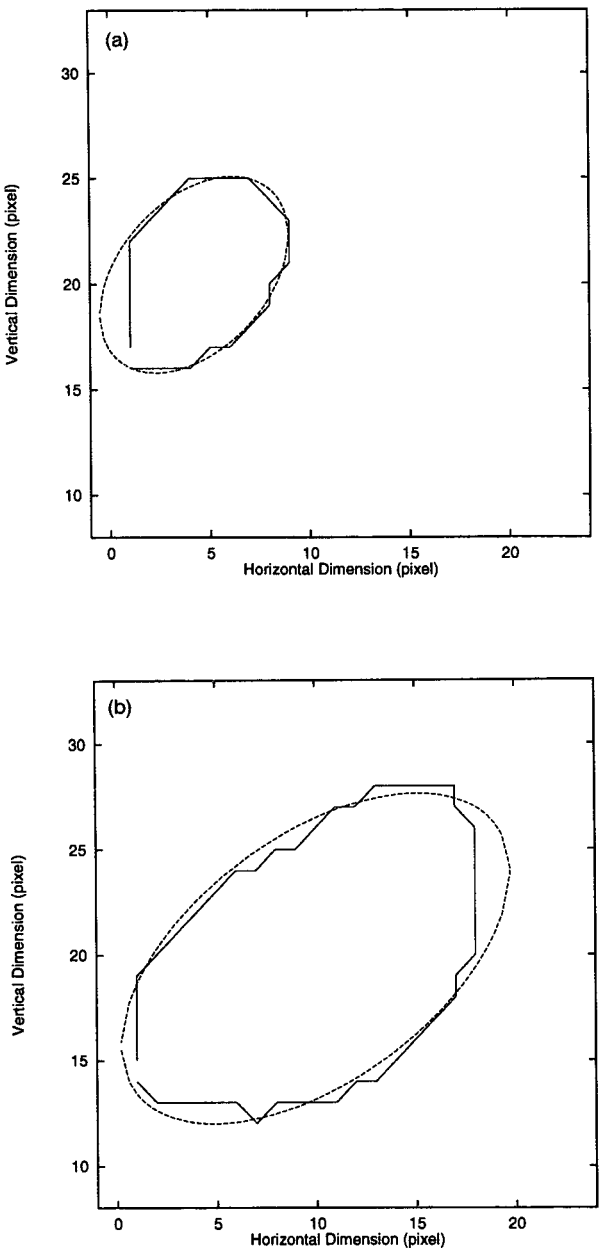

FIG. 6. Examples of ellipse-fitting results for full raindrop images: solid line is the contour of 2D-P raindrop image; dashed line is the ellipse-fitting result. (a) Small raindrop case. (b) Large raindrop case.

Figure 6 shows two examples of ellipse-fitting results for full raindrop images, where Fig. 6a shows the ellipse-fitting result for a small raindrop with horizontal dimension less than ten pixels, whereas Fig. 6b shows the ellipse-fitting result for a large raindrop with horizontal dimension close to 20 pixels. The dataset used for comparative study of the various techniques were collected by the Wyoming King Air on 8 August 1991 within moderate to intense showers during the CaPE field program. About 1000 2D-PMS full raindrop images were used as the test dataset. Parameters estimated for the images included the major axis a, minor axis b, axis ratio r, and the canting angle α (for partial images, the center coordinates were also estimated). These images were first processed by Fourier descriptor method and moment descriptor method, separately, to obtain the above parameters. Then they were processed using the ellipse-fitting algorithm given in section 2 to estimate the same parameters. Subsequently, the axis ratio and the volume equivalent spherical diameter D_{eq} (Bringi et al. 1984) of raindrops were computed based on these image parameters. Figure 7 shows the scatterplots between the Fourier descriptor results and ellipse-fitting results. Figure 7a is a scatterplot of D_{eq} of raindrops obtained from ellipse-fitting and Fourier descriptor methods. Figures 7b–c are similar to Figure 7a, except they show the raindrop axis ratio and the apparent canting angle, respectively. We note here that these apparent canting angles are not true canting angle of raindrops and refer to Chandrasekar et al. (1988) for details.

To get some idea about the statistical difference, we compute the bias and the root-mean-squared error (rmse) of the comparison between the Fourier descriptor method and the ellipse-fitting algorithm, as summarized in Table 1. From this table, it is obvious that the results of the ellipse-fitting algorithm agree well with the results of Fourier descriptor method.

b. Ellipse-fitting techniques for partial raindrop images

Fourier descriptor and moment descriptor techniques need the complete contour for processing and neither technique will work for partial images. However, the ellipse-fitting technique introduced in this paper can be applied to process partial raindrop images. Figure 8 shows two examples of ellipse fitting results for partial raindrop images. Figure 8a shows the ellipse-fitting result for a partial raindrop image with top part truncated, whereas Fig. 8b shows the ellipse-fitting result for a partial raindrop image with bottom part truncated.

The performance of ellipse-fitting technique for processing partial images was evaluated by the following procedure. First, the ellipse-fitting procedure was applied to the full raindrop images to estimate all parameters of the image, such as the center coordinates, the major and minor axes, and the canting angle as well as the volume equivalent spherical diameter D_{eq} of the raindrop. Subsequently, the top or the bottom of each image was truncated by a certain amount (20%, 30%, and 50% of the height) to generate a partial image test dataset, and then the partial ellipse-fitting algorithm was used to estimate all parameters once again. By comparing these two pairs of results, we were able to evaluate how well the ellipse-fitting method works for partial images.

In Fig. 9, the estimates of the ellipse center coordinates from full and partial raindrop images are given. Figure 9a shows a scatterplot of the X coordinates of the ellipse center obtained from full images and partial images with 20% truncation. Figure 9b shows the comparison of the Y coordinates of the ellipse center for the same dataset as used in Fig. 9a. Similarly, the X and Y coordinates were also estimated for partial raindrop images with 30% and 50% truncation and compared with the estimates obtained from the full images. Figure 10 shows the comparison of D_{eq} of raindrops obtained from full raindrop images and partial images with 20% truncation. The D_{eq} of raindrops were also computed from partial raindrop images with 30% and 50% truncation, respectively.

TABLE 1. Statistics of comparison between FD and ellipse fitting for full raindrop images.

Statistics	D_{eq} (mm)	Axis ratio r	Canting angle α (°)
Bias	0.14	0.045	1.4
rmse	0.16	0.075	4.2

The bias and rmse of the comparison between the estimates from full images and partial images were computed and summarized in Table 2. From the re-

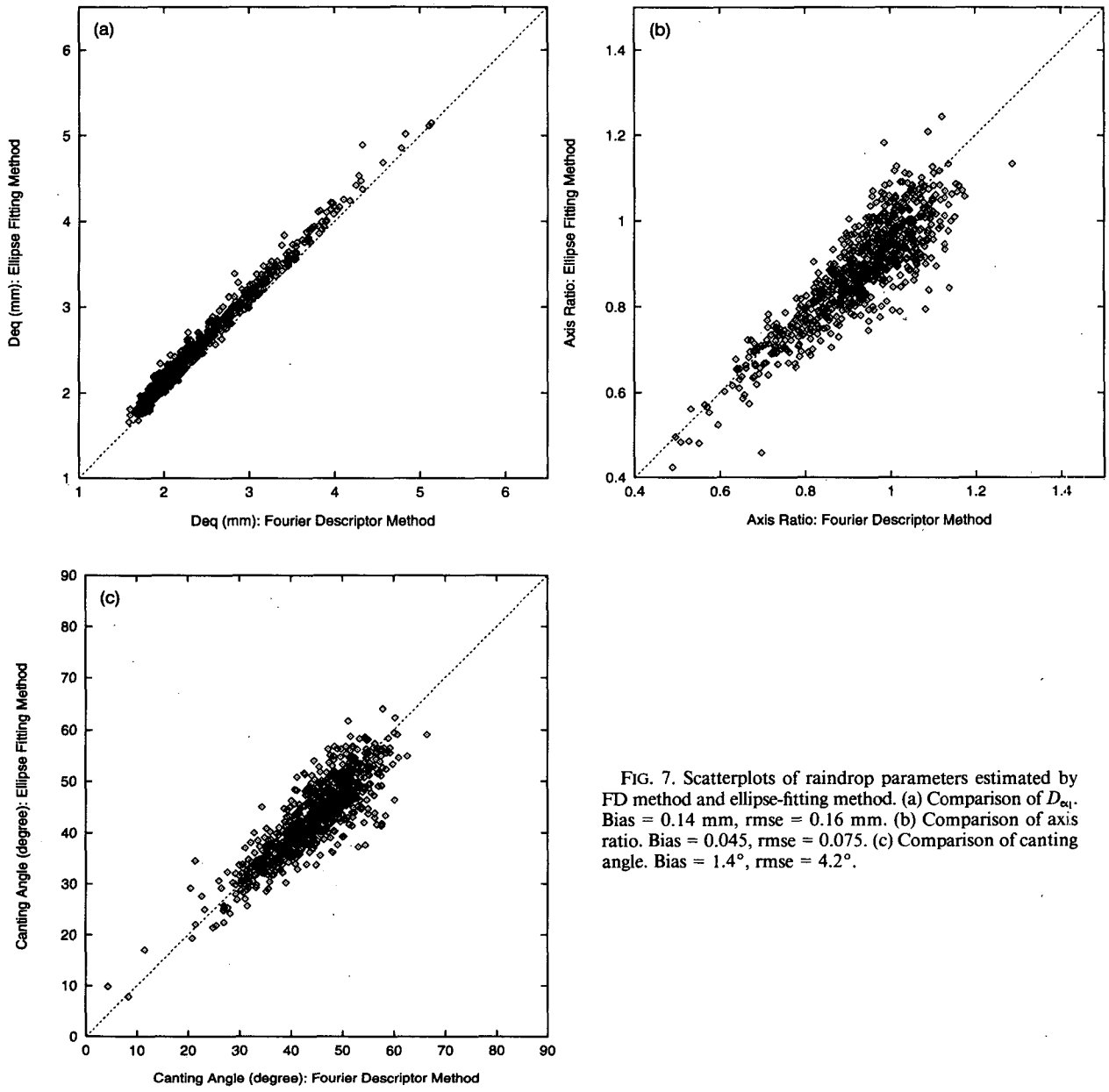

FIG. 7. Scatterplots of raindrop parameters estimated by FD method and ellipse-fitting method. (a) Comparison of D_{eq}. Bias = 0.14 mm, rmse = 0.16 mm. (b) Comparison of axis ratio. Bias = 0.045, rmse = 0.075. (c) Comparison of canting angle. Bias = 1.4°, rmse = 4.2°.

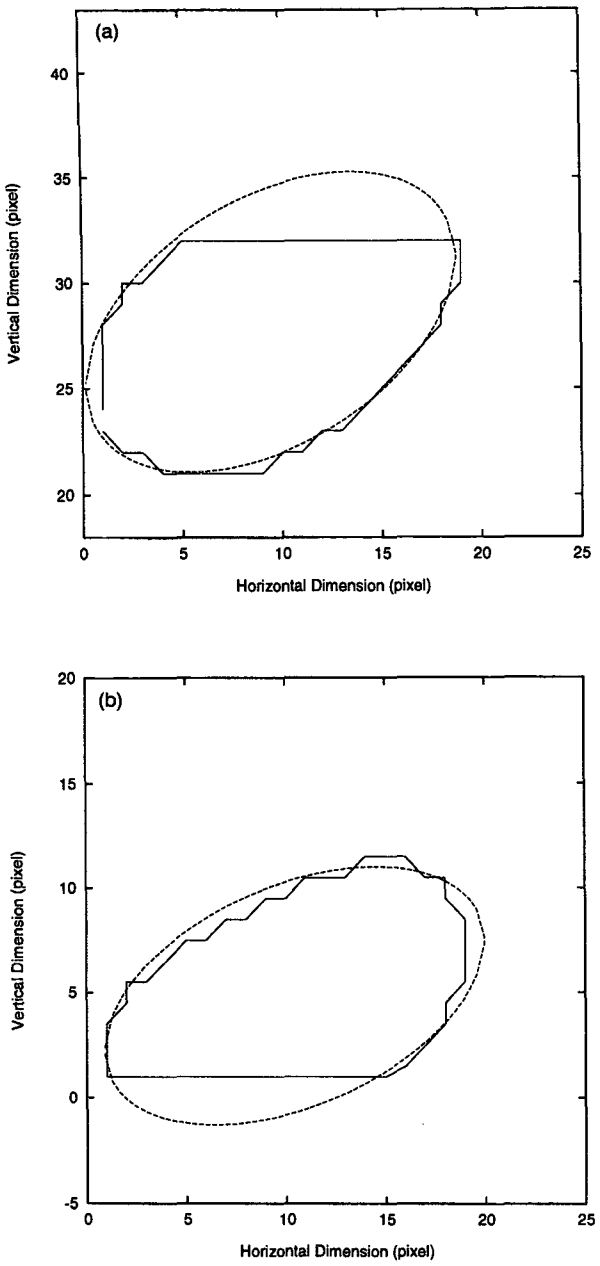

FIG. 8. Examples of ellipse-fitting results for partial raindrop images: solid line is the contour of the partial raindrop image and the dashed line is the ellipse fit. (a) Top part of the original image is truncated. (b) Bottom part of the original image is truncated.

sults of Table 2, we can see that the ellipse-fitting technique is very robust in locating the center of an ellipse, even when the raindrop image is cut off by 50%. Also, the estimates of D_{eq} from partial images match the estimates obtained from full images very well. This indicates that the D_{eq} estimates obtained from partial raindrop images is fairly accurate up to 50% truncation.

We note here that the main application of this technique in the context of partial images is to estimate the D_{eq} and the center coordinates (for drop size concentration computations). Axis ratio and canting angle estimated from partial raindrop images have a high standard error due to limited contour points. We do not recommend the application of the ellipse-fitting technique to estimate accurately the shape and orientation of raindrops from partial raindrop images.

4. Raindrop concentration and size distribution

One of the main objectives of the ellipse-fitting technique is to take into account the partial raindrop images in the computation of concentration and DSD. If we ignore partial images at the edge of the probe-sampling region, the uncertainties in the calculation of the concentration and other related quantities will increase, especially for larger size drops. The ellipse-fitting technique developed here was applied to the 2D-PMS data collected by the Wyoming King Air during the CaPE on 8 August 1991. Partial 2D-PMS raindrop images in the scan area were processed first by estimating the center coordinates using the ellipse-fitting method. Then the estimates of the center coordinates were used to check whether the center was located inside the sampling region of the optical array probe or not. If the center of a partial image was inside, then the particle was included in the DSD and concentration estimates. If the center was outside, the particle was excluded. Figure 11 shows the drop size concentration estimates using the procedure discussed above. The DSD shown in Fig. 11 corresponds to a flight path of approximately 45 s (1351:00–1351:45 EST). The corresponding sampling volume was 11.56 m^3. Of all the partial raindrop images that were examined, 290 were included in the DSD computation. The radar reflectivity Z_H and differential reflectivity Z_{DR} estimated from this DSD spectrum agree fairly well with the simultaneous radar measurements along the same flight track. Thus, based on the analysis procedures developed in this paper, we can use side-looking aircraft PMS data in rain to study the evolution of DSD, as well as the shape of hydrometeors that could be used in conjunction with polarimetric radar observations.

5. Summary and conclusions

An ellipse-fitting technique is introduced in this paper to process side-looking raindrop images that are sampled by the optical array 2D-PMS probe. The algorithm conforms to the natural data collection process, and therefore it is readily applicable to the parallel scan lines that are used to construct a 2D-PMS image. This technique is tested by first fitting full raindrop images and comparing against the results from Fourier descriptor method. This comparison shows that the results of the ellipse-fitting procedure agree well with

the Fourier descriptor and moment descriptor methods. Then the ellipse-fitting procedure is tested by fitting partial raindrop images generated by truncating the top part or the bottom part of full images, while at the same time the full images are also processed using the ellipse-fitting algorithm. It is shown that estimates of D_{eq} and the center location of raindrops can be estimated fairly accurately for partial images up to 50% truncation. The ellipse-fitting technique is shown to be an alternate tool besides the existing Fourier descriptor and moment descriptor methods for processing full 2D-PMS raindrop images, more importantly, it works successfully for partial raindrop images for which both the Fourier descriptor and moment descriptor methods cannot be used. It is also demonstrated that the ellipse-fitting procedure can be successfully used in evaluating the DSD of rain from side-looking 2D-PMS images. Though the technique was developed primarily for application with raindrop images, the algorithm can be extended to the analysis of nonspherical hydrometeor images.

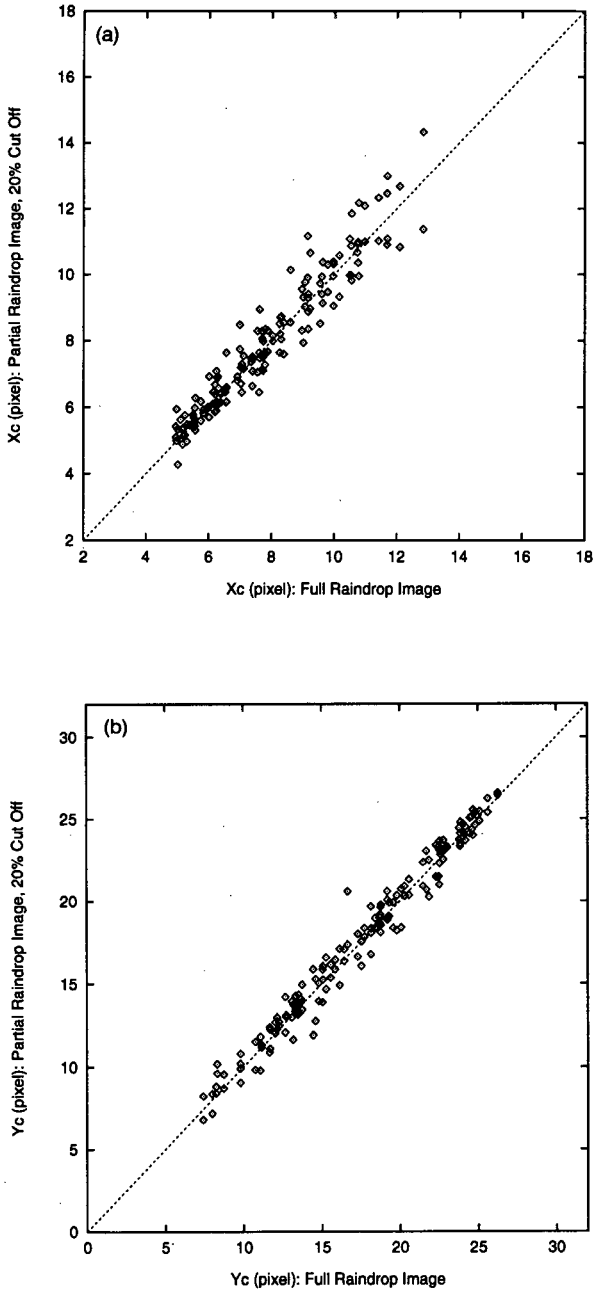

FIG. 9. Estimates of ellipse center coordinate (x_c, y_c) from partial images compared against the center coordinates obtained from full raindrop images. (a) X coordinate of the center, partial raindrop image with 20% truncation. Bias = 0.09 pixel, rmse = 0.60 pixel. (b) Y coordinate of the center, partial raindrop image with 20% truncation. Bias = 0.14 pixel, rmse = 0.83 pixel.

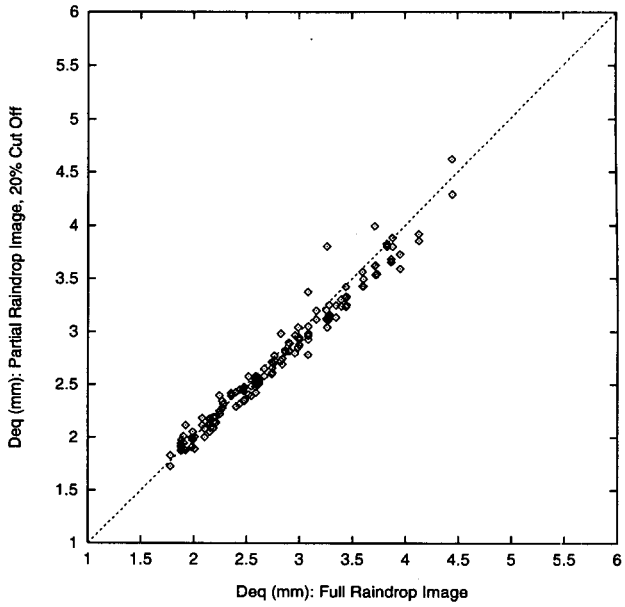

FIG. 10. Scatterplot of D_{eq} for full raindrop image versus partial raindrop images. Partial raindrop image with 20% truncation. Bias = 0.05 mm, rmse = 0.12 mm.

Acknowledgments. The authors acknowledge useful discussions with Professor V. N. Bringi of Colorado

TABLE 2. Statistics of comparison between estimates from full and partial raindrop images.

Truncation	Statistics	x_c (pixel)	y_c (pixel)	D_{eq} (mm)
20%	Bias	0.09	0.14	0.05
	rmse	0.60	0.83	0.12
30%	Bias	0.10	0.27	0.10
	rmse	0.68	1.09	0.21
50%	Bias	0.10	0.41	0.26
	rmse	1.00	1.81	0.34

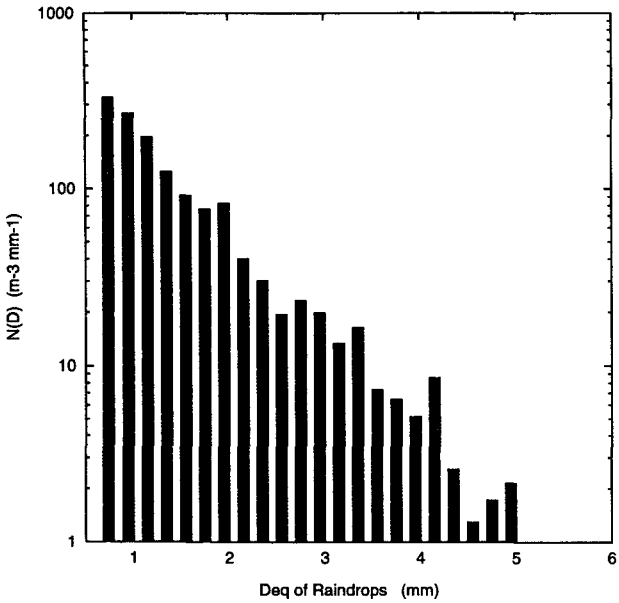

FIG. 11. Drop size distribution obtained from side-looking 2D-P images using ellipse-fitting algorithm. The data were collected by Wyoming King Air during 1351:00–1351:45 EST 8 August 1991, CaPE, Florida.

State University. This research was supported by the National Science Foundation (ATM-9200761).

APPENDIX

Formulas to Estimate the Parameters of an Ellipse

a. The center of the ellipse

The coordinates $(x_1, y_1), (x_2, y_2)$ on the ellipse satisfy the following equations: (Fig. 2)

$$\frac{[(x_1 - x_c)\cos\alpha + (y_1 - y_c)\sin\alpha]^2}{a^2} + \frac{[(x_1 - x_c)\sin\alpha - (y_1 - y_c)\cos\alpha]^2}{b^2} = 1 \quad \text{(A1)}$$

$$\frac{[(x_2 - x_c)\cos\alpha + (y_2 - y_c)\sin\alpha]^2}{a^2} + \frac{[(x_2 - x_c)\sin\alpha - (y_2 - y_c)\cos\alpha]^2}{b^2} = 1. \quad \text{(A2)}$$

Subtracting (A1) from (A2) and reordering the result, we get

$$r^2 = \frac{b^2}{a^2} = \frac{\tan\alpha - k_3}{1 + k_3\tan\alpha}\frac{s_1 - \tan\alpha}{1 + s_1\tan\alpha}, \quad \text{(A3)}$$

where

$$k_3 = \frac{y_{c1} - y_c}{x_{c1} - x_c}. \quad \text{(A4)}$$

Note s_1 and (x_{c1}, y_{c1}) are defined in section 2b. By the same approach, we have following equation from points $(x_3, y_3), (x_4, y_4)$,

$$r^2 = \frac{b^2}{a^2} = \frac{\tan\alpha - k_4}{1 + k_4\tan\alpha}\frac{s_2 - \tan\alpha}{1 + s_2\tan\alpha}, \quad \text{(A5)}$$

where

$$k_4 = \frac{y_{c2} - y_c}{x_{c2} - x_c}. \quad \text{(A6)}$$

From section 2b, we have $s_1 = s_2$. Comparing (A3) with (A5), it can be seen that $k_3 = k_4$, which implies that points (x_{c1}, y_{c1}), (x_{c2}, y_{c2}) and the ellipse center (x_c, y_c) are on the same line. The slope of this line is k_3 or k_4. From the definition of k_1 in section 2b, we have $k_1 = k_3 = k_4$. Similarly, we can show that

$$k_5 = \frac{y_{c3} - y_c}{x_{c3} - x_c} = k_6 = \frac{y_{c4} - y_c}{x_{c4} - x_c}. \quad \text{(A7)}$$

According to the definition of k_2 in section 2b, we have $k_2 = k_5 = k_6$. Therefore, points (x_{c5}, y_{c5}), (x_{c6}, y_{c6}) are also on the same line with the ellipse center (x_c, y_c). Since we have $k_1 \neq k_2$, the line defined by points (x_{c1}, y_{c1}), (x_{c2}, y_{c2}), (x_c, y_c) and the line defined by points (x_{c5}, y_{c5}), (x_{c6}, y_{c6}), (x_c, y_c) must have an intersection point, and this point is (x_c, y_c). Subsequently, x_c and y_c are given by Eqs. (9) and (10) in section 2b.

b. Estimates of axis ratio and canting angle

For an ellipse centered at origin (see Fig. 3), the general equation for a canted ellipse is simplified as

$$\frac{(x_s\cos\alpha + y_s\sin\alpha)^2}{a^2} + \frac{(x_s\sin\alpha - y_s\cos\alpha)^2}{b^2} = 1. \quad \text{(A8)}$$

Consider a vertical line that crosses points (x_{s1}, y_{s1}), (x_{s2}, y_{s2}) with $x_{s1} = x_{s2}$ on the contour of the ellipse, we can find a relation between y_{s1}, y_{s2}, and x_{s1} (or x_{s2}) using above equation as

$$y_{s1} + y_{s2} = \frac{x_{s1}(a^2 - b^2)\sin 2\alpha}{a^2\cos^2\alpha + b^2\sin^2\alpha}. \quad \text{(A9)}$$

Similarly, for a horizontal line crossing points (x_{s5}, y_{s5}), (x_{s6}, y_{s6}) with $y_{s5} = y_{s6}$ on the ellipse, we can find a relationship between x_{s5}, x_{s6}, and y_{s5} (or y_{s6}) as

$$x_{s5} + x_{s6} = \frac{y_{s5}(a^2 - b^2)\sin 2\alpha}{a^2\sin^2\alpha + b^2\cos^2\alpha}. \quad \text{(A10)}$$

Using (A9), (A10), we get the following equations:

$$\frac{x_{s1}}{y_{s1} + y_{s2}} + \frac{y_{s5}}{x_{s5} + x_{s6}} = \frac{a^2 + b^2}{(a^2 - b^2)\sin 2\alpha} \quad \text{(A11)}$$

$$\frac{x_{s1}}{y_{s1} + y_{s2}} - \frac{y_{s5}}{x_{s5} + x_{s6}} = \frac{\cos 2\alpha}{\sin 2\alpha}. \quad \text{(A12)}$$

Let d_1, d_2 be defined as

$$d_1 = \frac{x_{s1,s2}}{y_{s1} + y_{s2}} \tag{A13}$$

$$d_2 = \frac{y_{s5,s6}}{x_{s5} + x_{s6}}. \tag{A14}$$

We can solve for α and r from (A11), (A12) to get

$$\alpha = \frac{1}{2}\tan^{-1}\left(\frac{1}{d_1 - d_2}\right) \tag{A15}$$

$$r = \frac{b}{a} = \left[\frac{(d_1 + d_2)\sin 2\alpha - 1}{(d_1 + d_2)\sin 2\alpha + 1}\right]^{1/2}. \tag{A16}$$

REFERENCES

Beard, K. V., and C. Chuang, 1987: A new model for the equilibrium shape of raindrops. *J. Atmos. Sci.*, **44,** 1510–1524.

Bringi, V. N., T. A. Seliga, and W. A. Cooper, 1984: Analysis of aircraft hydrometeor spectra and differential reflectivity (Z_{DR}) radar measurements during the Cooperative Convective Precipitation Experiment. *Radio Sci.*, **19,** 157–167.

Chandrasekar, V., W. A. Cooper, and V. N. Bringi, 1988: Axis ratios and oscillations of raindrops. *J. Atmos. Sci.*, **45,** 1324–1333.

——, Y. Golestani, J. Turk, and V. N. Bringi, 1990: Fourier and moment methods applied to two-dimensional raindrop images. *J. Atmos. Oceanic Technol.*, **7,** 197–205.

Cooper, W. A., 1980: Estimation of rainfall using measurements from aircraft. *Third Conf. on Weather Modification,* WMO, Geneva, Switzerland, 365–372.

Duroure, C., 1982: Une nouvelle methode de traitement des images d'hydrometeores donnees par les sonde bidimensionnelles. *J. Rech. Atmos.*, **6,** 71–84.

Heymsfield, A. J., and J. L. Parrish, 1979: Techniques employed in the processing of particle size spectra and state parameter data obtained with the T-28 aircraft platform. NCAR/TN-137+IA. [Available from National Center for Atmospheric Research, Boulder, CO, 80307.]

——, and D. Baumgardner, 1985: Summary of a workshop on processing 2-D probe data. *Bull. Amer. Meteor. Soc.*, **66,** 437–440.

Hunter, H. E., R. M. Dyer, and M. Glass, 1984: A two-dimensional hydrometeor machine classifier derived from observed data. *J. Atmos. Oceanic Technol.*, **1,** 28–36.

Knollenberg, R. G., 1981: Techniques for probing cloud microstructure. *Clouds, Their Formation, Optical Properties, and Effects.* P. V. Hobbs and A. Deepak, Eds., Academic Press, 15–89.

Rahman, M. M., E. A. Quincy, R. G. Jacquot, and M. J. Magee, 1981: Feature extraction and selection for pattern recognition of two-dimensional hygrometeor images. *J. Appl. Meteor.*, **20,** 521–535.